Metabolic tuning of inhibition regulates hippocampal neurogenesis in the adult brain

Xinxing Wang[a], Hanxiao Liu[a], Johannes Morstein[b], Alexander J. E. Novak[b], Dirk Trauner[b], Qiaojie Xiong[a,1], Yuguo Yu[c,d,e,f,1], and Shaoyu Ge[a,1]

[a]Department of Neurobiology & Behavior, State University of New York at Stony Brook, Stony Brook, NY 11794; [b]Department of Chemistry, New York University, New York, NY 10003; [c]State Key Laboratory of Medical Neurobiology, School of Life Science, Fudan University, 200433 Shanghai, China; [d]Human Phenome Institute, Fudan University, 200433 Shanghai, China; [e]Research Institute of Intelligent and Complex Systems, Fudan University, 200433 Shanghai, China; and [f]Institute of Science and Technology for Brain-Inspired Intelligence, Fudan University, 200433 Shanghai, China

Edited by Mu-ming Poo, Chinese Academy of Sciences, Shanghai, China, and approved August 26, 2020 (received for review April 1, 2020)

Hippocampus-engaged behaviors stimulate neurogenesis in the adult dentate gyrus by largely unknown means. To explore the underlying mechanisms, we used tetrode recording to analyze neuronal activity in the dentate gyrus of freely moving adult mice during hippocampus-engaged contextual exploration. We found that exploration induced an overall sustained increase in inhibitory neuron activity that was concomitant with decreased excitatory neuron activity. A mathematical model based on energy homeostasis in the dentate gyrus showed that enhanced inhibition and decreased excitation resulted in a similar increase in neurogenesis to that observed experimentally. To mechanistically investigate this sustained inhibitory regulation, we performed metabolomic and lipidomic profiling of the hippocampus during exploration. We found sustainably increased signaling of sphingosine-1-phosphate, a bioactive metabolite, during exploration. Furthermore, we found that sphingosine-1-phosphate signaling through its receptor 2 increased interneuron activity and thus mediated exploration-induced neurogenesis. Taken together, our findings point to a behavior-metabolism circuit pathway through which experience regulates adult hippocampal neurogenesis.

adult hippocampal neurogenesis | neurocircuit | metabolic regulation | tetrode recording

In the adult brain, the hippocampus recruits several thousand new dentate granule cells (DGCs) into existing neural circuits on a daily basis (1–6). Decades of research suggest that this DGC recruitment is required for the normal cognitive function of hippocampal neural pathways (7–14). However, the mechanisms underlying hippocampal control of neurogenesis in response to external stimuli remain poorly understood.

Hippocampal neurogenesis is actively regulated by many hippocampus-engaged behaviors (15–20). Several lines of evidence demonstrate that both intrinsic and extrinsic signaling pathways are activated during hippocampus-engaged behaviors. For example, several studies show that these behaviors up-regulate metabolic factors, such as circulating insulin-like growth factor-1, vascular endothelial growth factor, and locally released fibroblast growth factor-1, and thereby regulate experience-induced neurogenesis (21–23). Several other studies suggest that neurogenesis is regulated by neurotransmitters that are locally released in response to neurogenic behaviors (24–26). Thus, both inhibitory and stimulatory activity mediated by neurotransmitter and metabolic signals, such as GABA and growth factors, may increase in response to behavioral stimuli and serve to regulate newborn neuron survival (22, 27–30). Although these studies provide mechanistic insights into neurogenic control, it remains poorly understood whether and how these molecular mechanisms govern hippocampal neurogenesis.

Recent evidence suggests that cellular network circuitry in the dentate gyrus regulates neurogenesis (31–33). How signals emanating from behavioral stimuli interface with the dentate gyrus neural network and control neurogenesis remains a central question. Post hoc analysis of c-fos expression and in vivo Ca^{2+} imaging show that DGCs are more active during hippocampal-engaged behaviors (8, 34, 35), which may be essential for experience-induced neurogenesis (35), although the effect of DGC activation on neurogenesis is debated (36–39). However, stimulation or inhibition of inhibitory interneurons in the dentate gyrus is reported to stimulate or inhibit hippocampal neurogenesis, respectively (21, 40–42). As such, despite elegant advances in elucidating relevant cellular and molecular components in the dentate gyrus, it remains unclear to what extent and through which mechanisms hippocampal microcircuitry responds to behavioral neurogenic stimuli and how such circuit engagement impacts the neurogenic niche.

Here, to investigate how the adult mouse brain actively reacts to behavioral stimuli and regulates hippocampal neurogenesis, we employed physiological and metabolomic techniques to interrogate the impact of contextual exploration on dentate gyrus circuitry and neurogenesis. We identified a sphingosine-1-phosphate (S1P)-S1P receptor 2 (S1PR2) signaling pathway that mediates inhibitory tuning of dentate gyrus circuitry during exploratory behavior. The activation of this axis was necessary for the exploration-induced survival of newborn DGCs. Combined with computational modeling, we determined that the neurogenic capacity of the dentate gyrus is heavily dependent on the circuit's excitatory–inhibitory balance under different behavioral conditions.

Significance

Our the brain actively responds to changes in the environment by remodeling neural circuits. One important aspect of neuroplasticity is adult neurogenesis, which involves the generation, survival, and incorporation of new neurons into existing circuits and is unique to two discrete areas of the mammalian brain. The hippocampus, critical for learning and memory, is one such area that exhibits ongoing neurogenesis throughout an individual's lifetime. Although recent studies have confirmed that hippocampal behaviors regulate neurogenesis, the mechanistic pathways governing that regulatory activity remain poorly understood. In this work, we found that hippocampal behaviors increase inhibitory circuit activity through a metabolic pathway, and established a computational model to quantitively model the relationship between circuit activity and control of hippocampal neurogenesis.

Author contributions: X.W., Q.X., Y.Y., and S.G. designed research; X.W. and H.L. performed research; J.M., A.J.E.N., and D.T. contributed new reagents/analytic tools; X.W. and Y.Y. analyzed data; and X.W., Q.X., and S.G. wrote the paper.

The authors declare no competing interest.

This article is a PNAS Direct Submission.

[1]To whom correspondence may be addressed. Email: qiaojie.xiong@stonybrook.edu, yuyuguo@fudan.edu.cn, or Shaoyu.ge@stonybrook.edu.

This article contains supporting information online at https://www.pnas.org/lookup/suppl/doi:10.1073/pnas.2006138117/-/DCSupplemental.

First published September 24, 2020.

Results

Hippocampus-Engaged Exploration Increases Inhibition and Decreases Excitation in the Dentate Gyrus. To determine how hippocampal-engaged behaviors regulate adult neurogenesis, we employed experimental and computational modeling techniques to examine how neural circuitry in the dentate gyrus responds to experiences to in turn regulate neurogenesis.

Exploration in a context, such as an enriched environment (EE), increases adult hippocampal neurogenesis primarily by promoting the survival of newborn DGCs. Therefore, we examined neural circuit activity in the dentate gyrus during exploration by employing tetrode recording to analyze neuronal firing in the dentate gyrus of freely moving adult mice in an EE. Two weeks after tetrode implantation, we recorded neuronal activity when a mouse was in its home cage (HC) with only bedding material for 30 min, and when it explored a similar cage but with four to six novel objects (EE) for 30 min (Fig. 1*A*). We classified recorded units as DGCs or interneurons according to their waveform symmetry index, waveform width, and long-term firing rate (43–45) (Fig. 1 *B* and *C* and *SI Appendix*, Fig. S1). We then analyzed firing frequency over time and across HC and EE conditions. Of more than 250 units, 40% of DGCs showed an increased firing rate during exploration, whereas the remaining predominantly showed a decreased firing rate (Fig. 1 *D* and *E*). In contrast to DGCs, 60% of interneurons substantially increased their firing rate during exploration (Fig. 1 *D* and *E*).

These results were substantiated when the firing units of DGCs and inhibitory neurons were globally averaged. We found that the average DGC firing rate was unchanged during the first 2 min, gradually decreased during the next 3 min (*SI Appendix*,

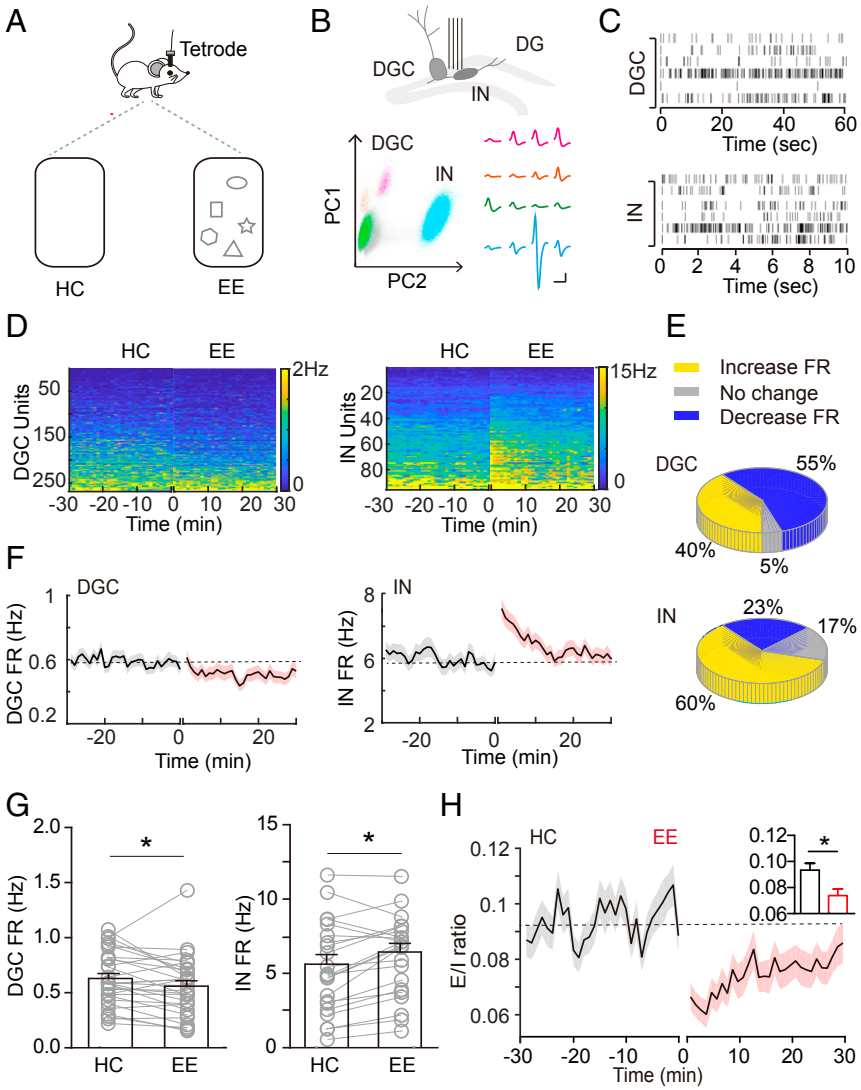

Fig. 1. Activation of inhibitory and suppression of excitatory neural circuits in the dentate gyrus during hippocampus-engaged exploration. (*A*) Schematic drawings showing tetrode implantation and behavior conditions. (*B*) Schematic drawings showing the method of distinguishing between excitatory and inhibitory neurons: (*Upper*) tetrode implantation in the dentate gyrus; (*Lower*) representative waveforms of three DGC units and one interneuron (IN) unit. (Scale bar, 5 mV and 10 ms.) (*C*) Raster plots of DGC and IN unit activities. (*D*) Heatmaps representing the firing rate of individual units in HC and EE conditions. Units are sorted by their average 30-min firing rate during HC recording. (*E*) Distribution of DGCs and INs based on their average firing rate (FR). Average FR in the EE condition was defined as an "increase" or "decrease" when it changed by ≥5% relative to that in the HC condition, whereas "no change" was defined as change of <5%. (*F*) Change in average FR of all excitatory ($n = 265$; mice = 3) and inhibitory ($n = 95$; mice = 3) units over time. (*G*) Average FR of excitatory and inhibitory units in HC and EE conditions (*$P < 0.05$; RM-ANOVA). (*H*) E/I ratio in HC and EE conditions, calculated as f_{EX}/f_{IN}. Black lines indicate the mean value, and shaded areas indicate the SEM. Dashed gray line is the averaged E/I ratio of HC recording. *$P < 0.05$; RM-ANOVA.

Fig. S2*A*), and remained decreased over the remaining recording time (Fig. 1 *D*, *F*, and *G*). In contrast, the average firing rate of interneurons during exploration was robustly increased, although this increase declined over the 30 min of recording (Fig. 1 *D*, *F*, and *G*). To extend these analyses, we found that the amount of burst firing, another important feature of neuronal activity, was decreased for DGCs but increased for interneurons (*SI Appendix*, Fig. S2*B*). Moreover, both DGCs and interneurons began to change their firing rate starting at the beginning of EE (*SI Appendix*, Fig. S2*C*), and their changes in activity were closely correlated in the EE condition (*SI Appendix*, Fig. S2*D*). In addition, the altered firing returned to baseline over 1 h (*SI Appendix*, Fig. S3*A*). This firing pattern is similar to our previously observed exploration-induced increase in blood flow (21). When mice were returned to their home cages, neuronal firing promptly returned to baseline levels (*SI Appendix*, Fig. S3 *B* and *C*), further suggesting that the increased firing rate was EE-induced. Video-tracking analyses indicated that animals had similar locomotion in the HC and EE conditions (*SI Appendix*, Fig. S4 *A–C* and Movies S1 and S2). Of interest, we found that 5 of 26 interneurons had a weak correlation between firing rate and locomotion, suggesting a heterogeneity of interneurons in the EE condition (*SI Appendix*, Fig. S4 *D* and *E*).

GABAergic interneurons in the dentate gyrus exert inhibitory control over DGCs via feedback or feedforward inhibition (46–49). To assess a possible pattern of activity changes, both excitatory and inhibitory changes were analyzed as an excitation-to-inhibition (E/I) ratio in the dentate gyrus circuit during exploration (Fig. 1*H*). We found a substantial decrease in E/I rate during exploration, suggesting a more pronounced inhibitory environment in the dentate gyrus.

Taken together, our findings reveal that during exploration, excitation in the dentate gyrus is dampened and inhibition is increased, suggesting a determining role of relative changes in

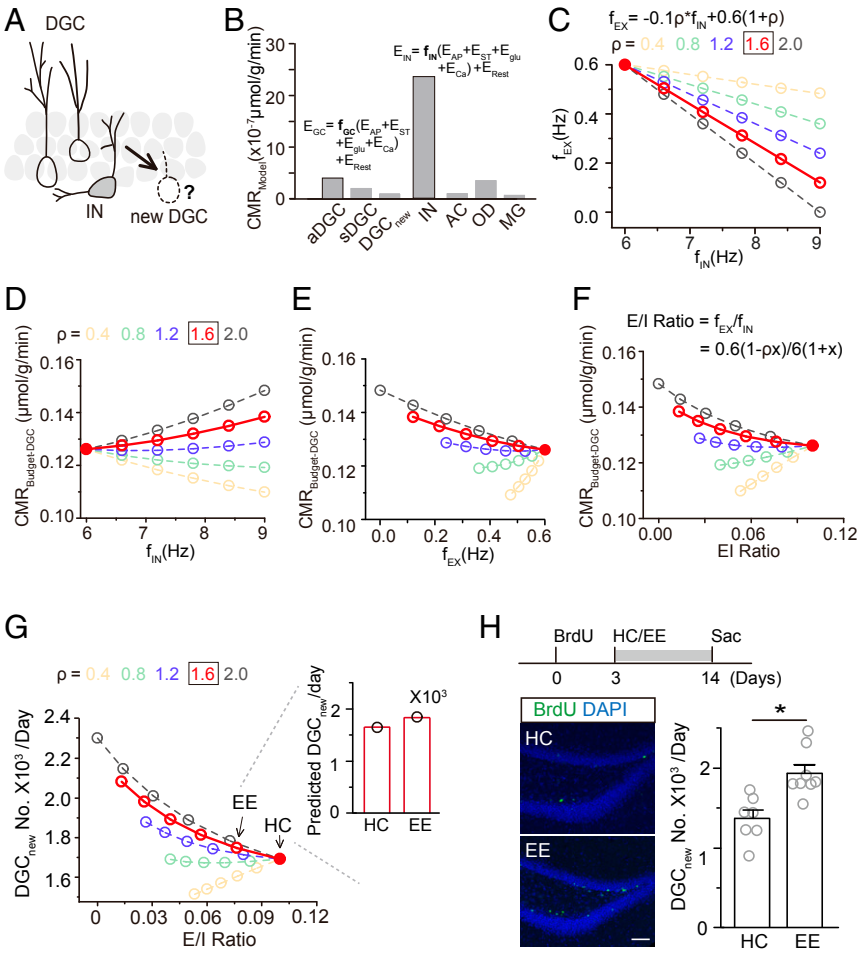

Fig. 2. Computed neural circuit activity in the dentate gyrus predicts experience-induced hippocampal neurogenesis. (*A*) Schematic drawing of the hypothesis that local dentate gyrus neural circuitry, including DGCs and interneurons (INs), regulates the survival of newborn neurons. (*B*) Modeled glucose oxidization of cerebral metabolic rate (CMR) for each major cell type in the dentate gyrus considering the cost of action potentials (E_{AP}), synaptic transmission (E_{ST}), glutamate or GABA recycling (E_{glu}), calcium entry into neurons (E_{Ca}), and cell maintenance (i.e., resting potential and housekeeping metabolic consumption, E_{Rest}). Active granule cells (aDGC, firing rate = 0.6 Hz), silent granule cells (sDGC, firing rate = 0.06 Hz), and newborn DGCs (DGC_{new}) were classified as the excitatory (EX) population. GABAergic neurons were classified as the inhibitory (IN) population. Astrocytes (AC), oligodendrocytes (OD), and microglia (MG) were classified as the glial population. (*C*) Relationship between IN and EX activity. The firing rate of interneurons (f_{IN}) was calculated as $6(1 + x)$ and of excitatory neurons (f_{EX}) was calculated as $0.6\ (1 - \rho x)$. Here, x is the percentage change in the firing rate, whose decrease is proportional to an increase in the inhibitory firing rate with a scale quantified by the variable ρ, which was set to 0.4, 0.8, 1.2, 1.6, or 2. (*D–F*) Relationships between the energy budget for DGCs and IN activity (*D*), EX activity (*E*), and the E/I ratio (*F*). (*G*) Relationship between the number of new DGCs/d and E/I ratio. The *Inset* shows the predicted number of newborn neurons based on the E/I ratio. Arrows indicate E/I ratios in HC and EE conditions. The firing rate of interneurons was 6.0 and 6.8 Hz and of DGCs was 0.59 and 0.51 Hz in HC and EE conditions, respectively. (*H*) Representative images of ~14-d-old $BrdU^+$ newborn DGCs. (Scale bar, 50 μm.) (*Right*), numbers of new DGCs labeled by one-time BrdU injection (HC, $n = 7$; EE, $n = 8$; $^*P < 0.05$; paired t test).

activity state in regulating exploration-induced hippocampal neurogenesis.

Computational Modeling Characterizes the Relationship between Excitatory–Inhibitory Activity and Neurogenesis in the Dentate Gyrus. Our observation of marked exploration-induced inhibitory tuning of the dentate gyrus raises the question of whether this has a role in exploration-induced neurogenesis. As with other neural processes, neurogenesis is an energetically demanding task and depends on the energy economy of the dentate gyrus (50, 51). We thus hypothesized that the tuning of excitatory–inhibitory activity in the dentate gyrus impacts the overall energy available for newborn DGCs.

We used a computational approach to model the relationship between neural circuit activity and the survival of newborn DGCs (Fig. 2*A*) based on the energy homeostasis principle over the long term. At any given time, the adult brain is considered homeostatic in energy metabolism (52, 53). However, the energy consumption of neurons is affected by their firing rate (54–56), suggesting that the brain dynamically redistributes energy to carry out a variety of specific cognitive or metabolic functions. From this perspective, we sought to test the hypothesis that exploration-induced inhibitory tuning creates an energetically favorable scenario for neurogenesis. We thus aimed to establish a model to calculate the energy redistribution in the dentate gyrus that occurs during exploration and its possible relationship with neurogenesis.

The dentate gyrus is mainly composed of excitatory neurons, interneurons, and glial cells. We first computed cellular energy consumption in the dentate gyrus. As shown in *SI Appendix*, Table S1, based on the energy cost of maintaining membrane potential, action potential firing, synaptic transmission, and housekeeping, we established models to measure the energy consumption of individual cell types (Fig. 2*B* and *SI Appendix*). The energy consumption of the three major cell types was similar to that measured in actual samples (*SI Appendix*, Fig. S5*A*) (57, 58), suggesting the sufficiency of these models. The model showed that the energy consumption of excitatory and inhibitory neurons was highly correlated with their respective firing rates (Fig. 2*B* and *SI Appendix*). To calculate the effect of firing rates on energy distribution, we next established the relationship between the firing of interneurons and excitatory neurons considering that they impact each other (48, 59, 60). We defined the firing rate of interneurons as $6(1 + x)$, for which x is a variable vector. Due to the interplay between inhibitory and excitatory neurons in the dentate gyrus, the activity of DGCs was considered as $0.6(1 - \rho x)$, for which ρ is a constant. With different values of ρ, excitatory neurons show different responses to changes in interneuron activity (Fig. 2*C*). According to the firing rates of DGCs and interneurons (0.6 Hz for DGCs and 5.9 Hz for interneurons) recorded from the dentate gyrus under the HC condition, ρ is 1.6 for the dentate gyrus circuit in the adult mouse brain.

We next calculated how the firing of DGCs and interneurons influences energy consumption in the dentate gyrus. The total energy consumption rate in the dentate gyrus in the adult brain is ~0.42 μmol/g/min, of which 30% (0.126 μmol/g/min) is consumed by DGCs in the resting state (*SI Appendix*, Fig. S5*B*) (53, 54). Based on the energy consumption rate of interneurons and the relationship between inhibitory and excitatory neuron firing, we established the relationship between the firing rate of interneurons and energy consumption in the dentate gyrus (Fig. 2*D* and *SI Appendix*). Although elevated interneuron firing increased energy consumption, DGC consumption decreased due to enhanced inhibition. Interestingly, the total energy consumption of the interneuron and excitatory populations decreased in response to increased interneuron activity in the dentate gyrus with a ρ of 1.6. Therefore, excessive energy is generated in the dentate gyrus with higher levels of interneuron activity (Fig. 2*D*). Similarly, we established the relationship between the firing rate of DGCs and energy consumption, with model results suggesting that a higher DGC firing rate imposes higher energy demands from the dentate gyrus (Fig. 2*E* and *SI Appendix*, Fig. S5 *C* and *D*).

To establish a model including both DGCs and inhibitory neurons, we calculated the relationship between the E/I ratio and energy consumption in the dentate gyrus (Fig. 2*F* and *SI Appendix*, Fig. S5 *C* and *D*). In the resting state, the E/I ratio was 0.1, with an energy surplus to DGCs of 0.126 μmol/g/min (Fig. 2*F*). We further transformed the energy budget into predicted numbers of new DGCs based on correlations with energy redistribution and the E/I ratio (Fig. 2*G* and *SI Appendix*, Fig. S5 *E* and *F*).

We validated this model by assessing the number of newborn neurons in the EE condition. Exploration decreased the E/I ratio from 0.1 to 0.075 (DGCs from 0.59 to 0.51 Hz and interneurons from 5.99 to 6.81 Hz). The number of new DGCs was predicted to be 1,691 in the HC condition and 1,780 in the EE condition with a ρ of 1.6 (Fig. 2 *G*, *Inset*). To determine model accuracy, we counted the number of surviving new DGCs in HC and EE conditions (21, 35). A single injection of BrdU was used to label the surviving newborn neurons. We found that the number of surviving newborn neurons was similar to that obtained by model calculation (Fig. 2*H* and *SI Appendix*, Fig. S5*G*), suggesting that this model accurately predicts the number of new DGCs based on changes in neural circuit activity.

Altogether, we developed a computational model based on circuit activity-dependent energy consumption. Using biased circuit inhibition under exploration as an input to the model, we determined that an exploration-induced increase in inhibitory neuron firing leads to an increase in the number of newborn DGCs. Thus, exploration-induced inhibitory tuning of the dentate gyrus circuit facilitates an energetically economic environment for neurogenesis.

Metabolomic Profiling Reveals Augmentation of Sphingolipids during Exploration. Our results show that exploration inhibits neural circuit activity via an unknown mechanism. The sustained inhibition led us to speculate that the dentate gyrus may be controlled by metabolic principles and signaling pathways as a mouse explores. To identify metabolic and signaling changes, we profiled metabolites of the hippocampus under HC and EE conditions (Fig. 3*A*). Of a total of 593 metabolites, we found that many metabolites differed between conditions, including lipids, amino acids, and peptides (Fig. 3*B*). Of the metabolites with a significant difference ($P < 0.05$, unpaired t test) between EE and HC conditions, as shown in a hierarchical clustering heatmap and pie map (Fig. 3 *C* and *D*), lipids showed the most striking changes. To investigate these changes in more detail, we performed higher-resolution lipidomic analysis of the mouse hippocampus after 1 h of HC or EE and found a robust increase in several bioactive metabolites of the sphingosine pathway, including ceramides, dihydro-sphingosine-1-phosphate, sphingosine, and S1P (Fig. 3*E*). For a comparative control, we collected and profiled cortical tissues, which had similar sphingolipid levels between conditions (*SI Appendix*, Fig. S6), suggesting that sphingolipid levels were increased preferentially in the hippocampus.

Interneurons Express S1PR2, Whose Activation Causes Depolarization. The increased levels of several bioactive sphingolipids found by lipidomic analysis raised the possibility that these lipids play a role in the increased inhibitory circuit activity in the dentate gyrus during exploration. To assess this possibility, we examined whether an increase in hippocampal S1P influences neural circuit activity in the dentate gyrus. To specifically test the effect of S1P, not only a metabolite, on neural circuit activity, we employed a metabolically stable and photo-switchable analog of S1P (PhotoS1P). The metabolic stability of this analog is markedly increased and after an hour no degradation is observed. We performed whole-cell patch-clamp

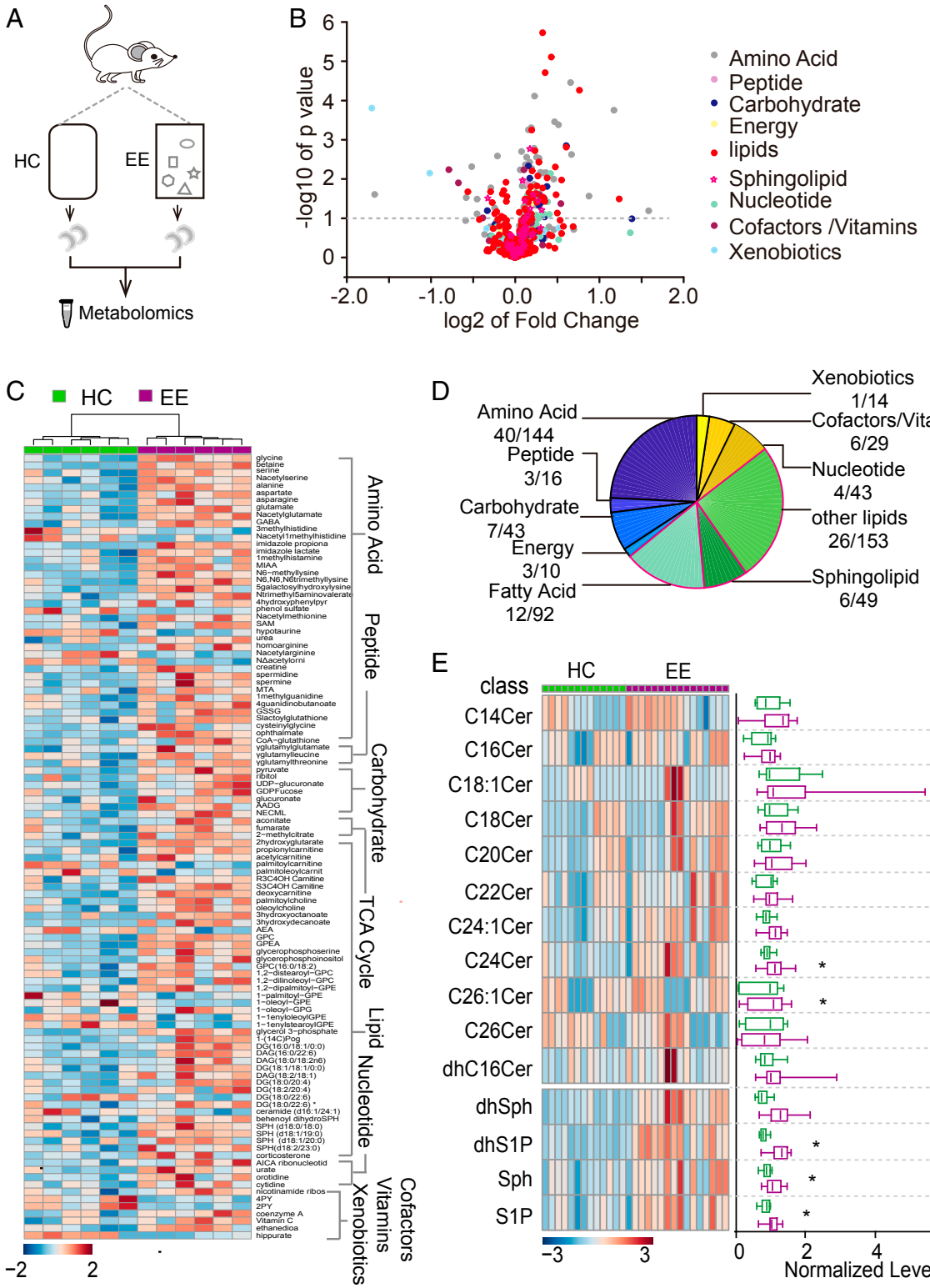

Fig. 3. Metabolomics and lipidomics analyses reveal an increase in bioactive metabolite S1P during hippocampus-engaged exploration. (*A*) Schematic drawing of the experimental design for metabolomic analysis. (*B*) Volcano plot showing the fold-change and *P* value for all 593 metabolites between HC and EE conditions. Lipids, including sphingolipids, showed extensive changes between conditions (HC, $n = 6$; EE, $n = 6$; $^*P < 0.05$; unpaired *t* test). (*C*) Hierarchical clustering heatmap showing metabolites with significant differences between HC and EE conditions grouped into seven major pathways. The lipid pathway was one of the primary pathways influenced by exploration. (*D*) Proportion of metabolites with significant differences ($P < 0.05$, unpaired *t* test) in each major pathway. (*E*, *Left*) Hierarchical clustering heatmap showing lipidomic analysis; (*Right*) mean values in HC and EE conditions (HC, $n = 13$; EE, $n = 16$; $^*P < 0.05$; unpaired *t* test).

recording of neurons in the dentate gyrus in acutely prepared hippocampal tissue in the presence of both glutamatergic and GABAergic inhibitors to block synaptic transmission. We found that 365-nm light illumination of S1P promoted the firing of interneurons but not DGCs (Fig. 4 *A*–*C*). Interestingly, this potentiation was abolished by treatment with JTE-013 (25 μM), an antagonist of S1PR2 (Fig. 4 *C*, *Right*). Thus, it appears that 365-nm light illumination of PhotoS1P specifically activates S1PR2 (61). We next assessed whether S1PR2 is expressed by dentate gyrus interneurons using immunostaining for S1PR2 and the interneuron-specific marker GAD67. As expected, S1PR2 was selectively expressed in most GAD67$^+$ neurons in the dentate gyrus but not newborn and mature DGCs (Fig. 4 *D* and *E* and *SI Appendix*, Figs. S7*A* and S11), suggesting preferential expression by interneurons. This preferential S1PR2 expression by interneurons was also seen in other brain areas, such as the olfactory bulb, cerebellum, and thalamic reticular nucleus (*SI Appendix*, Fig. S7*B*). These results suggest that S1PR2 plays a role in the specific activation of dentate gyrus interneurons.

To verify the S1PR2 activation of interneurons, we performed whole-cell patch-clamp recording of parvalbumin$^+$ (PV$^+$) neurons in a transgenic mouse line expressing the tdTomato reporter in PV$^+$ interneurons. We first confirmed that PV$^+$ neurons expressed S1PR2 (*SI Appendix*, Fig. S7*B*). To determine whether S1PR2 activation affects PV$^+$ neuron activity, we induced action potentials with and without application of the S1PR2-specific agonist CYM5520 (62). The application of CYM5520 (10 μM) significantly increased the number of spikes in these neurons (Fig. 4 *F* and *G*). To further test this apparent depolarizing effect, we measured membrane potentials and found that S1PR2 activation was accompanied by depolarized resting membrane potentials (Fig. 4*H*). In contrast, when we used JTE-013 to block endogenous S1P activation of S1PR2, PV$^+$ neurons were hyperpolarized, resulting in decreased spikes (*SI Appendix*, Fig. S7*C*). Importantly, S1PR2 activation had little effect on current-evoked action potentials in DGCs (*SI Appendix*, Fig. S7*D*).

In summary, these findings reveal that S1PR2 is preferentially expressed by dentate gyrus interneurons and that S1PR2 activation results in increased firing of interneurons, suggesting that S1P activation of S1PR2 on interneurons is involved in mediating regulatory inhibition of the dentate gyrus.

S1PR2 Activity Is Necessary for Exploration-Induced Inhibition in the Dentate Gyrus. Given that exploration increases hippocampal S1P and that increased S1PR2 activity leads to depolarization of interneurons, we speculated that S1P-S1PR2 signaling plays a role

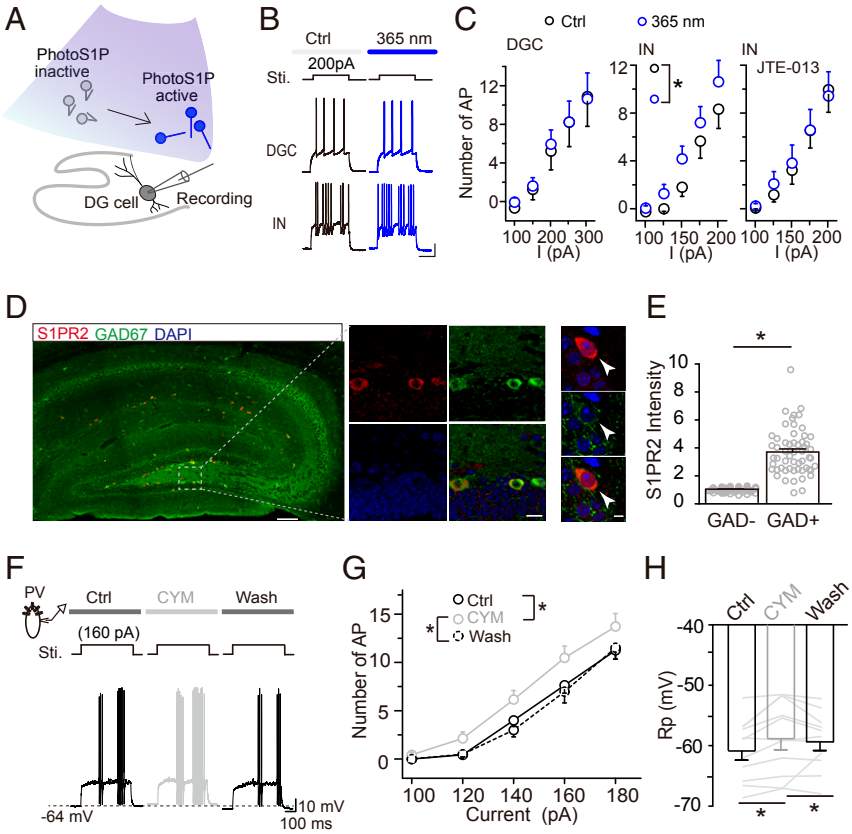

Fig. 4. S1PR2 is specifically expressed by interneurons, and its activation causes neuronal depolarization. (*A*) Schematic drawing showing the switch of nonfunctional PhotoS1P (inactive) to functional (i.e., active) PhotoS1P by UV light (365 nm) illumination during slice recoding. (*B*) Representative images showing that active PhotoS1P increased current-evoked action potentials of interneurons (INs) but not DGCs. (Scale bar, 20 mV and 200 ms.) (*C*) Effect of active PhotoS1P on current-evoked action potentials (APs) of DGCs and INs (*$P < 0.05$, two-way RM-ANOVA). (*Right*) IN activity when S1PR2 was blocked by its antagonist JTE-013 (25 μM). Bicuculline (20 μM) and CNQX (10 μM) were preapplied to block inhibitory and excitatory synaptic transmission. (*D* and *E*) Preferential expression of S1PR2 in the hippocampus (arrowheads point to typical interneurons in the subgranular zone acquired by high resolution scanning) (*D*) and quantification in interneurons and noninterneurons in the dentate gyrus. (Scale bars are 100, 10, and 2 μm from left to right.) Normalized S1PR2 fluorescence intensity of GAD67$^+$ vs. GAD67$^-$ cells (*$P < 0.05$; unpaired *t* test). Data were normalized to the averaged intensity of GAD67$^-$ cells (*E*). (*F*–*H*) Representative recordings and quantitative data showing current-evoked APs of PV$^+$ neurons before, during, and after activation of S1PR2 by perfusion of CYM5520 (10 μM). Activation of S1PR2 significantly depolarized resting membrane potential (Rp) (*$P < 0.05$; two-way/one-way RM-ANOVA). (Scale bar, 10 mV and 100 ms.)

in EE-induced inhibitory tuning and neurogenesis of the dentate gyrus in behaving mice. To test this possibility, we employed shRNA knockdown of S1PR2 in interneurons by creating an AAV9 virus to deliver shRNA against S1PR2 tagged with GFP (shS1PR2) to suppress S1PR2 expression. We used another AAV9 virus with scrambled shRNA tagged with GFP as a control (shCtrl). We verified the knockdown efficiency of shS1PR2 by analyzing S1PR2 expression in shS1PR2$^+$ neurons in the dentate gyrus and found an ~56% reduction compared with that in control neurons expressing shCtrl (Fig. 5*B*). To verify that S1PR2 knockdown affects S1PR2-mediated (i.e., CYM5520-induced) depolarization of interneurons, we recorded the firing of shS1PR2$^+$ interneurons (*SI Appendix*, Fig. S8). The addition of CYM5520 had little effect on firing (*SI Appendix*, Fig. S8*B*), suggesting that shS1PR2 decreased S1PR2 expression to a sufficient extent to prevent S1PR2-mediated interneuron activation.

These results suggested that we could use shS1PR2-mediated S1PR2 knockdown in dentate gyrus interneurons to test whether S1PR2 is involved in exploration-induced circuit activity changes in vivo. Two weeks after shS1PR2 injection and tetrode implantation in the dentate gyrus, we recorded neuronal activity under both HC and EE conditions (Fig. 5*A*). Similar to that seen in wild-type mice in the EE condition (Fig. 1*C*), interneurons in shCtrl-injected mice showed a substantially increased rate of firing during exploration compared with that seen in the HC condition (Fig. 5 *C–E*, *Left*, and *SI Appendix*, Fig. S9*A*). However, there was little increase in the firing rate of interneurons in shS1PR2-injected mice (Fig. 5 *C–E*, *Right*, and *SI Appendix*, Fig. S9*A*). These results suggest that S1PR2 is required for interneuron activation during exploration. Note that despite large variation in the average firing rates of DGCs (Fig. 5 *F–H* and *SI Appendix*, Fig. S9*B*), the average firing rate was slightly decreased during exploration in the shS1PR2 group. Our findings reveal that S1PR2 knockdown dampens exploration-induced inhibition of the dentate gyrus, suggesting a prominent role for this signaling pathway.

S1PR2 Activity Is Necessary for Exploration-Induced Survival of Adult-Born DGCs. To determine whether S1P-S1PR2 plays a role in regulating exploration-induced neurogenesis, we examined neurogenesis in shS1PR2-mediated S1PR2 knockdown mice, in which we also recorded DGC and interneuron activity. We calculated the E/I ratio in control and S1PR2 knockdown mice using the population firing rate recorded in HC and EE conditions (Fig. 6*A*). shCtrl mice showed a decreased E/I ratio during exploration. In contrast, S1PR2 knockdown suppressed the

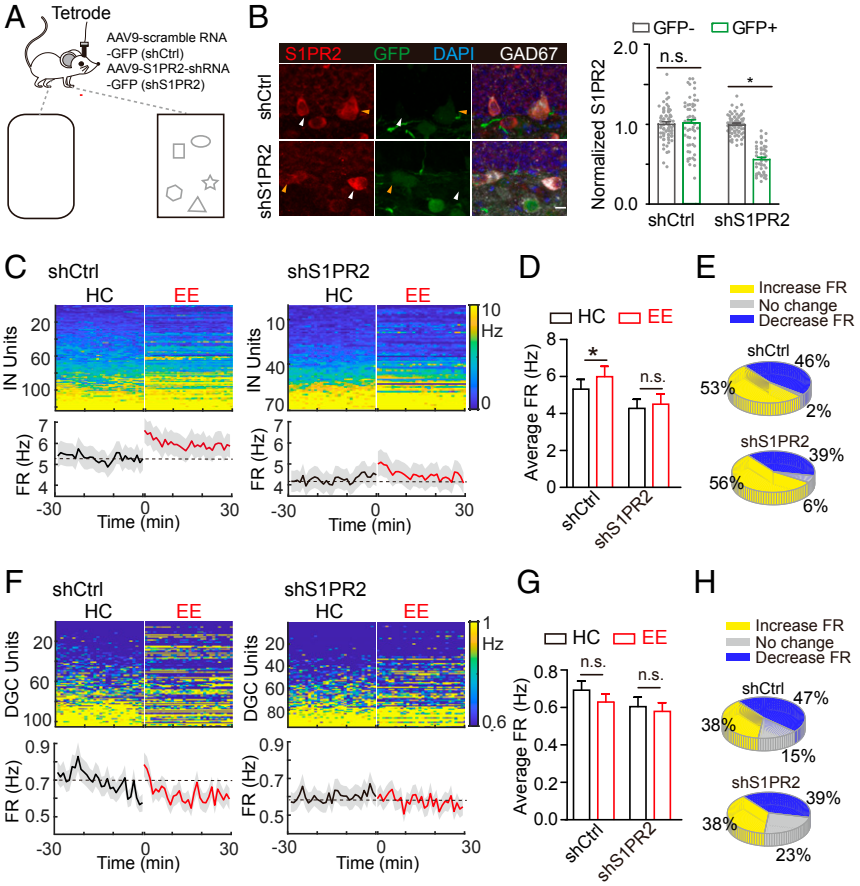

Fig. 5. S1PR2 activation is necessary for exploration-induced neurogenesis. (*A*) Schematic diagram showing the experiment design. shS1PR2 was injected into the dentate gyrus to manipulate expression of S1PR2. (*B*) Validation of the knockdown efficiency of shS1PR2: (*Left*) representative images; (*Right*) quantification of S1PR2 signal in GAD67$^+$ cells (shS1PR2, $n = 47$; shCtrl, $n = 55$; $^*P < 0.05$; unpaired t test). Typical analyzed infected and noninfected neurons are indicated by yellow and white arrowheads, respectively. Scale bar, 10 μm. (*C*) Heatmap showing firing rate (FR) of individual inhibitory (IN) units in HC and EE conditions after shS1PR2 ($n = 70$) or ShCtrl ($n = 123$) injection. Units were sorted by their average 30-min FR in the HC condition. (*Lower*) Average FR of all units in each condition. Dashed gray line is the average value in the HC condition. (*D*) Average FR of IN units in HC and EE conditions ($^*P < 0.05$; one-way ANOVA). (*E*) Distribution of increase, no change, and decrease in FR of INs. (*F*) Heatmap showing FR of individual DGC units in HC and EE conditions after shS1PR2 ($n = 95$) or shCtrl ($n = 104$) injection. (*G*) Average FR of DGC units in HC and EE condition (n.s., $P > 0.05$; one-way ANOVA). (*H*) Distribution of increase, no change, and decrease in FR of DGCs.

exploration-induced decrease in E/I ratio (Fig. 6*A*). We also found less neurogenesis in the shS1PR2 group compared with that in the shCtrl group (Fig. 6*B*). We estimated the number of newborn DGCs in the EE condition to be 1,626 and 1,525 for the shCtrl and shS1PR2 groups, respectively.

To investigate the role of S1PR2 in mediating the exploration-induced survival of newborn neurons, we examined newborn neuron survival with these two genetic manipulations (Fig. 6*C*). All mice were given a single BrdU injection 20 d after injection of shS1PR2 or shCtrl virus. We exposed mice to EE or HC conditions beginning the fourth day of BrdU injection (Fig. 6 *D* and *E*). Exploration increased the number of $BrdU^+$ neurons in shCtrl mice but did not significantly change the number of $BrdU^+$ neurons in shS1PR2 virus-injected mice (Fig. 6*E*). To rule out an effect of S1PR2 knockdown on the differentiation of neural progenitor cells, we examined NeuN and doublecortin (DCX) expression together with BrdU. We found that 94.6% of $BrdU^+$ cells were DCX^+ 14 d after labeling, suggesting no detectable effect on differentiation (Fig. 6*F*). Consistently, exploration had little effect on the number of DCX^+ cells in the shS1PR2 group, as was observed in shCtrl-injected mice (Fig. 6*G*). In summary, our findings reveal that S1PR2 expression in interneurons is indispensable for the exploration-induced survival of newborn neurons, suggesting the necessity of this metabolic pathway in behavior-dependent neurogenesis.

Discussion

Whether and how behaviors regulate neural circuits to influence neurogenesis have been largely unexplored. In this study, we found that exploration of an EE, which promotes hippocampal neurogenesis, preferentially activated interneurons, resulting in suppression of DGC activity. To understand how this change in circuit activity regulates neurogenesis, we developed a computational model to calculate the number of newborn DGCs generated based on neuronal firing rates. This model shows strong quantitative associations among the inhibitory/excitatory state, energy homeostasis, and the neuron-generating capacity of the dentate gyrus, consistent with our experimental findings. We further elucidated a mechanistic explanation of this relationship by discovering a cluster of bioactive metabolites, including S1P, that are increased by exploration. We found that S1P activation of S1PR2, which is highly expressed in interneurons, specifically up-regulates interneuron activity within dentate gyrus circuitry. Critically, we found that the S1P→S1PR2→inhibitory neuron signaling axis is necessary for exploration-induced inhibitory activity in the dentate gyrus and the resulting enhancement of

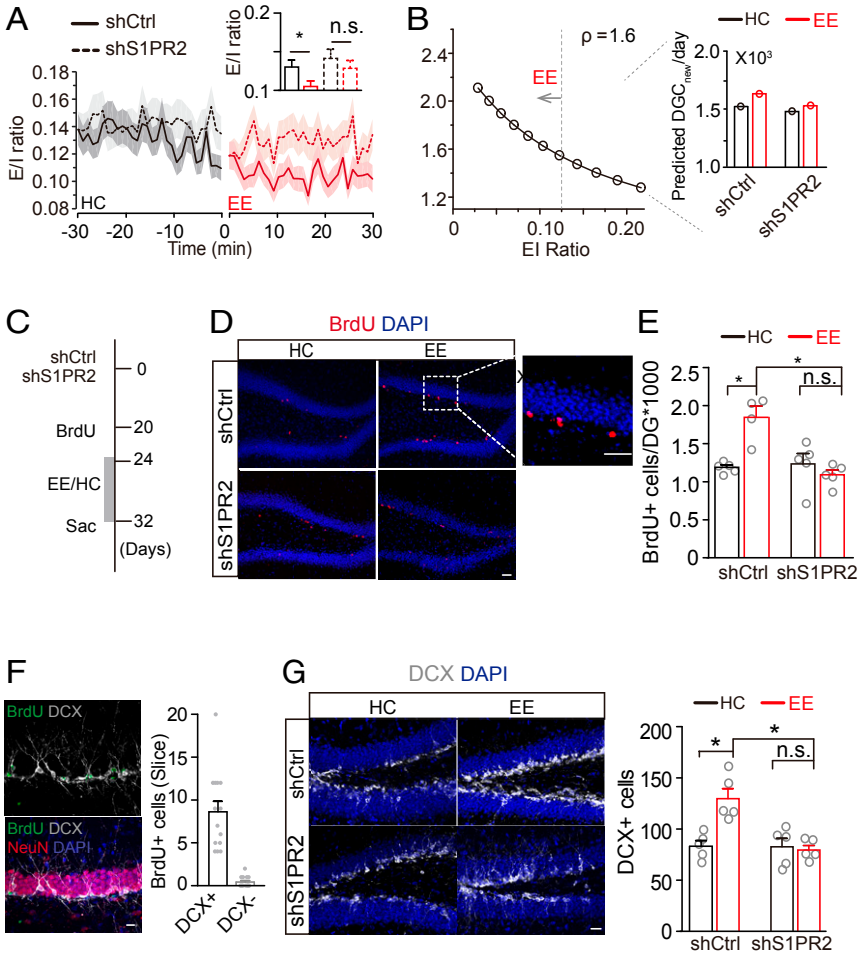

Fig. 6. S1PR2 activation is necessary for exploration-induced survival of adult-born DGCs. (*A*) E/I ratio in shS1PR2- and shCtrl-injected mice in HC and EE conditions. (*B*) Relationship between the number of new DGCs/d and E/I ratio; ρ was 1.6 based on the recordings depicted in Fig. 5 *C–F*. *Inset* plot shows the predicted number of newborn DGCs in shS1PR2- and shCtrl-injected mice. (*C*) Schematic diagram showing the experimental design. (*D* and *E*) Representative images of BrdU labeling and (*D*) and quantification of surviving new DGCs (n.s., $P > 0.05$; $^*P < 0.05$; unpaired *t* test) Scale bar, 50 μm. (*E*). (*F, Left*), verification that $BrdU^+$ cells are DCX^+; (*Right*) quantification of BrdU and DCX coexpression in the dentate gyrus. Scale bar, 10 μm. (*G, Left*) Representative images of DCX^+ cells; (*Right*) quantification of immature DGCs (n.s., $P > 0.05$; $^*P < 0.05$; unpaired *t* test). Scale bar, 20 μm.

neurogenesis. Together, our results identify a lipid metabolic signaling pathway, through which behavioral stimuli regulate hippocampal neural circuits and in turn control neurogenesis in the adult brain.

Hippocampal Neural Circuit Activity during EE Exploration. Hippocampus-engaged contextual exploration promotes neurogenesis (15, 21). Here, we investigated how neural circuits actively regulate neurogenesis in response to exploration. We observed an overall increase in the population of activated interneurons, as evidenced by an increased average firing rate (Fig. 1*G*). Accounting for this increase in interneuron activity, our measurements indicate that both burst firing (a more efficient mode of information transmission) (63) and tonic firing (nonburst firing) increased during exploration (*SI Appendix*, Fig. S2*B*). Correspondingly, excitatory DGCs showed decreases in these parameters (Fig. 1 *C* and *D* and *SI Appendix*, Fig. S2). Together, the changes in firing properties of interneurons and DGCs indicate that the excitatory and inhibitory balance shifts to a greater inhibitory state during EE condition.

The shift to a more inhibitory state may be interpreted in light of the distinct nature of dentate gyrus neural circuits. Due to both their intrinsic hyperpolarized membrane potentials and strong inhibitory inputs from GABAergic interneurons, DGCs typically exhibit a sparse firing rate (64–66). However, although DGCs are the main information processing units with the most afferent and efferent synaptic connections, only a small proportion of DGCs are activated at any given time (67). In this regard, strong inhibition may serve to select a small and distinct population of mature DGCs and amplify differences in signals from similar patterns of inputs, which would contribute to pattern separation, an important function of the dentate gyrus (68). The average firing rate of DGCs showed a short period of resistance followed by a sustained decrease during exploration (Fig. 1*F*) and the firing of DGC and interneurons were closely correlated (*SI Appendix*, Fig. S2 *C* and *D*), suggesting that the decrease might arise from locally enhanced inhibition. This enhanced feedback inhibition would ensure a high spike threshold for DGCs, which is important for sparse coding or decorrelated population activity (69). Increased inhibition may facilitate the addition of newborn neurons by allowing the availability of more energy under homeostasis (Fig. 2). In this study, we performed a short-term tetrode recording under the EE condition and found that the increase in interneuron firing declined after the initial peak. This should be interpreted in the context of our previous study, which indicated that exploratory behaviors of animals in EEs are rhythmic and dynamic over long time scales (21), suggesting that the circuit activities change in a periodic manner and thus support the long-term effects of EE on neurogenesis.

We note that we did not dissect different classes of interneurons in this study. However, based on previous studies showing that PV^+ interneurons play a major role in regulating neurogenesis (21, 40, 41), we expect that these neurons are important players. Previous studies of the primary visual cortex indicated that vasoactive intestinal polypeptide-expressing interneurons respond to locomotion (70). Our locomotion analysis indicated that animals had locomotion activities during the HC and EE recording sessions (*SI Appendix*, Fig. S4 *A*–*C*). Moreover, only a few neurons showed a weak correlation between firing and locomotion activity (*SI Appendix*, Fig. S4 *D* and *E*). These results suggest that the increase in interneuron population activity may partially result from vasoactive intestinal polypeptide-expressing interneurons. Future in-depth analyses and experiments are required to further elucidate specific interneuron contributions.

Ambiguity of Neural Circuit Activity in Hippocampal Neurogenesis. An abundance of evidence suggests that newborn DGCs are necessary for normal hippocampal function (7, 10, 13, 71–74). Newborn DGCs are excitatory neurons, and during the process of circuit integration these cells receive increased inhibition from local interneurons (75) and compete with preexisting mature DGCs for inputs from the neural circuitry (20, 76, 77).

How is the number of newborn DGCs precisely controlled? One would expect that the circuitry behavior of mature adult DGCs is a deciding factor. For example, elimination of mature DGC spines promotes the integration of newborn neurons (77). Conversely, manipulation of the number of immature granule cells alters the synaptic functioning of mature DGCs (76). Furthermore, regulation of newborn neuron activity changes the overall number and activity of active mature DGCs (8, 78). These results suggest that DGC activity plays a role in controlling the number of newborn DGCs, and hence maintaining energy homeostasis and proper hippocampal function. However, conflicting evidence suggests that exploration increases DGC activity (using c-fos as reporter), with a corresponding increase in neurogenesis. However, in the present study, tetrode recording in freely moving mice revealed an increase in the activity of inhibitory interneurons before a DGC population change toward decreased activity (*SI Appendix*, Fig. S2*A*), suggesting that interneurons drive the inhibition of DGC activity during exploration. These results are further supported by specific optogenetic activation of PV^+ interneurons, which also promoted the survival of newborn DGCs (*SI Appendix*, Fig. S10*C*).

Optogenetic intervention of either excitatory or inhibitory dentate gyrus circuits could affect hippocampal neurogenesis (*SI Appendix*, Fig. S10). In particular, the number of survived newborn neuron was similar when mice were kept under of a consistent condition (*SI Appendix*, Fig. S10*A*). Activation of mature DGC activity by optogenetic stimulation decreased the survival of newborn neurons (*SI Appendix*, Fig. S10*B*). However, activation of PV^+ interneurons could increase the survival of newborn neurons (*SI Appendix*, Fig. S10*C*). To explain relationships among interneuron activation, DGC inhibition, and the promotion of neurogenesis, we modeled relationships between the E/I ratio and survival of newborn DGCs (Fig. 2*G*). Neuronal activities, including generating action potentials to relay and process inputs, account for 50 to 80% of the total energy expenditure (54, 55). Remarkably, total brain energy consumption increases proportionally with the number of neurons across species, including humans (53). These findings suggest that energy availability critically restricts the ensemble and function of neural circuitry (52). Although neurons have a highly specialized system for managing their energy demands, such as neurovascular coupling that provides phasic regulation of energy supply (21, 79, 80), several lines of evidence indicate that it is reasonable to assume a constant value of energy availability for a neural circuit over the long term. Neurons require a minimum amount of energy to stay alive and maintain a steady amount of free ATP to achieve homeostasis (81, 82). One would expect that continuously recruited new DGCs increase the total number of active neurons in the dentate gyrus and thus increase the demand for energy. The coding of information by neurons is a high-energy process due to the existence of background noise and demand for information precision. Theoretical studies suggest that neural circuits apply a general rule to maintain energy-efficient coding by optimizing the number of neurons in the network necessary for maximal information coding with minimal energy cost (83, 84). For example, sparse coding, in which only a small fraction of neurons are active at any one time (67, 85), is proposed as a mechanistic solution to the limited energy availability to neurons (54, 86). Thus, the sparse coding and low excitability properties of DGCs may provide solutions to the energy constraints of homeostasis (54, 87), allowing the dentate gyrus to continue recruiting new neurons into the circuit.

Mechanisms of Enhanced Experience-Induced Inhibition. Neurogenesis is a process in which the hippocampus must balance increased energy consumption with homeostasis (52, 53). Thus, we suspect that exploration-induced neurogenesis necessitates reorganization of the energy budget of different cell types in the dentate gyrus. We found a robust enhancement of inhibitory neuron activity in the dentate gyrus accompanied by a slight decrease of excitatory DGC activity. Considering the multiple inputs to interneurons, including those from local DGCs and long projections from outside the hippocampus (88, 89), exploration-induced inhibition of DGCs may have multiple local or remote drivers. Here, we found that activation of a sphingolipid signaling pathway mediated EE-induced inhibition (Fig. 3 *C* and *E*). The EE also provides motor and sensory stimulations; but, although we did observe a significant change in the hippocampus during EE, there was no such change in the visual cortex (Fig. 3*E* and *SI Appendix*, Fig. S6). The mechanism of this hippocampus-specific change of S1P in the EE is unclear. It is possible that exploration was more reliant on hippocampal activity. Increase in S1P induced by exploration highlights the potential function of bioactive lipids in regulating interneuron activity and influencing neurogenesis. Previous study indicated that S1PR2 is expressed in the hippocampus and modulates the long-term potentiation (90). However, our immunostaining and electrophysiological recording data showed that S1PR2 is highly expressed in interneurons of the dentate gyrus and has a significant effect on interneuron activity (Fig. 4). Our experiment, in which we costained with immature neuron marker DCX and S1PR2, indicated that newborn and mature DGCs rarely expressed S1PR2 (*SI Appendix*, Fig. S11), which rules out the direct modulation of newborn neurons through the S1P-S1PR2 pathway. We found that S1PR2-knockdown interneurons exhibited similar physiological properties in response to stimulation (*SI Appendix*, Fig. S8), suggesting that the intrinsic properties of interneurons likely remain unchanged. We should point out that in addition to S1PR2, S1PR1, and S1PR3 also regulate neuronal excitability (91, 92), and our previous study indicated that S1PR1 could regulate the maturation of newborn neurons (93). However, our immuno-localization results (Fig. 4*D* and *SI Appendix*, Fig. S7*A*) indicate that S1PR1 and S1PR3 have unique expression patterns but not specifically in interneurons, suggesting differences in their overall impact on circuits rather than the specific modulation of interneurons in the hippocampus. The cellular mechanisms underlying S1PR2-induced stimulation of interneurons is not presently known. Although activation of S1PR2 increases cAMP levels in smooth muscle cells (94), the mode of S1PR2 signaling in neurons remains to be elucidated.

Pathways for GABAergic Stimulation of Neurogenesis. We and others previously found that newborn DGCs richly express GABA receptors. The activation of these receptors by ambient GABA levels is necessary for normal neurogenesis, survival, and integration (41, 42, 73). We recently showed that GABAergic neurons control local blood vessel dilation and impact neurogenesis (21), further suggesting a role of metabolic regulation. Despite such advances in understanding how neural circuits regulate neurogenesis, there remains a dearth of information about how behaviors regulate neural circuits that further impact neurogenesis. In this study, we discovered that the S1P-S1PR2 signaling axis mediates increased neurogenesis in response to hippocampus-engaged behaviors by regulating dentate gyrus neural circuitry within the framework of energy homeostasis.

Methods and Materials

Animals. All experimental procedures were carried out in accordance with guidelines from the National Institutes of Health and approved by the Stony Brook University Animal Care and Use Committee. The mouse lines used were C57BL/6 mice (Charles River Laboratories) and PV-Cre [B6; 129P2-Pvalbtm1(cre)Arbr/J] and Ai14 [B6; 129S6-Gt(ROSA)26Sortm14(CAG-tdTomato)Hze/J] mice (Jackson Laboratory). Mice were housed under a 12-h light/dark cycle and given ad libitum access to food and water.

Tetrode Implantation and Recording. For recording from freely moving mice, we implanted a custom-made tetrode in the dorsal dentate gyrus. The tetrode array contained eight tetrodes (consisting of four polyimide-coated nichrome wires [wire diameter 12.7 μm; Kanthal Palm Coast] twisted together and gold-plated to an impedance of 0.3 to 0.5 MΩ at 1 kHz) and was mounted on a vertically movable microdrive (43). The tetrode array was sterilized with 70% ethyl alcohol and positioned in the upper granule cell layer of the dorsal dentate gyrus (AP = −2.0, ML = 1.3, DV = 1.5 mm) after removal of the dura. A small anchoring stainless screw (shaft diameter: 0.86 mm; length: 4 mm; Fine Science Tools) was driven into the bone above the cerebellum to serve as a reference electrode. Finally, the tetrode array was cemented to the skull using dental acrylic, with the reference cable passing through the cement. After 1 wk of recovery, mice were familiarized with the recording environment three times. The tetrode was then lowered down to the dentate gyrus after each recording with close monitoring (about 40 μm/time). After the last recording, all mice were killed for confirmation of tetrode implantation. For S1PR2 knockdown and control mice, AAV9-S1PR2-shRNA-GFP and AAV9-luciferase shRNA-GFP virus (Abcam) were injected into the dentate gyrus of 6-wk-old C57BL/6 mice. Tetrodes were implanted 2 wk after virus injection.

Mice were placed in the recording room for adaption to the environment 30 min before recording. Continuous recording was performed when mice were in their home cage and then gently transferred to a new cage with four to six novel objects and bedding material. During the entire tetrode recording procedure, video was recorded to monitor mouse behavior. After each recording, tetrodes were lowered, and the next recording was performed every other day. Single unit signals from the dorsal dentate gyrus were amplified and digitized using Cheetah Data Acquisition (Neuralynx). Signals were filtered at 600 to 6,000 Hz, and offline analysis was used to separate action potentials of single units (43). Briefly, single units were identified by grouping similar waveforms based on two principal components, peak and valley. Final clusters were manually selected (MClust-4.4; A. D. Redish, University of Minnesota, Minneapolis, MN) based on waveform similarity and autocorrelograms. The average waveform of each channel was measured, and the channel with the largest peak-to-valley amplitude was used to generate the peak-to-valley spike width. A waveform symmetry index was calculated as the ratio of peak amplitude to valley amplitude for all units. For each unit, firing rate during the entire recording session was calculated to serve as the long-term firing rate. All isolated single units were classified based on their waveform symmetry ratio, spike width, and long-term firing rate (*SI Appendix*, Fig. S1). In line with prior studies, we classified units with a low long-term firing rate and low burst index as DGCs from excitatory units (95, 96). For each unit, an average firing rate in the EE condition >105% or <95% of that in the HC condition was defined as an increase or decrease, respectively, and an average firing rate between these two boundaries was defined as no change. Burst firing was determined by counting the number of spikes with intervals <10 ms within each burst.

Energy Budget and Neurogenesis Modeling. To model the energy metabolism of the dentate gyrus, we first calculated the energy consumption of individual cell types. Three major types of cells—excitatory neurons, interneurons, and glial cells—were considered. The energy metabolism for each cell type was calculated based on multiple parameters, including maintenance of membrane resting potentials, action potential conduction, synaptic transmission, glutamate or GABA recycling, and presynaptic calcium entry into neurons (*SI Appendix*) (97). This metabolic budget model for the adult mouse dentate gyrus was validated by comparing the calculated total dentate gyrus metabolic cost with its actual experimental measurement. We constructed a mathematical model bridging the dentate gyrus metabolic budget and available energy surplus allowing for the maximal number of surviving DGCs. The total energy budget for the dentate gyrus included contributions from the demands of excitatory neurons (energy cost E_e), inhibitory cells (E_i), and glial cells (E_g).

$$E_{DG} = E_e + E_i + E_g \quad [1]$$

E_e, E_i, and E_g were calculated as follows:

$$E_e = N_{DGC}E_{DGC} + N_{MC}E_{MC} + N_{DGC0}E_{DGC0}$$
$$E_i = N_{IN}E_{IN} \quad [2]$$
$$E_g = N_{AC}E_{AC} + N_{OD}E_{OD} + N_{MG}E_{MG}.$$

The numbers of each cell type are provided in the *SI Appendix*. The dynamics of competition and cooperation between excitation and inhibition determine the activity levels of excitatory and inhibitory neurons. The simplified equation for the dentate gyrus budget model was:

$$E_{DG} = d_1 + d_2 f_e + d_3 f_i, \quad [3]$$

where d_1, d_2, and d_3 were calculated as 5.887×10^{14}, 2.47×10^{14}, and 3.7103×10^{13} (ATP/s), respectively (*SI Appendix*). The total budget for the dentate gyrus in 1-y-old adult mice was 9.6×10^{14} (ATP/s), which is equal to a 0.42 (μmol/g/min) glucose oxidation rate. The glucose oxidation rate for excitatory cells, inhibitory neurons, and glial cells was 0.249, 0.108, and 0.063 μmol/g/min, respectively (*SI Appendix*, Fig. S5*A*). These results were determined to be consistent with actual metabolic measurements through validation against measured anatomical morphology and biophysical parameters of DGCs in previous studies (*SI Appendix*).

To model neurogenesis based on energy budget, we propose that the inhibitory firing rate, f_i, directly modulates the excitatory firing rate, f_e, according to the following equation:

$$f_i = f_i^0(1 + x)$$
$$f_e = f_e^0(1 - \rho x), \quad [4]$$

where f_i^0 and f_e^0 are the base firing rates of inhibitory and active excitatory DGCs, respectively. Here, $f_e^0 = 0.6$ Hz and $f_i^0 = 6$ Hz based on our experimental recordings. The number of DGCs, N_{DGC}, was determined by:

$$E_{DG} = c_1 + c_2 f_e + c_3 f_i + N_{DGC}(a_1 + 0.127 b_1 f_e)$$
$$c_1 = N_{DGC0}a_1 + N_{MC}a_2 + N_{IN}a_3 + N_{AC}a_4 + N_{OD}a_5 + N_{MG}a_6$$
$$c_2 = 0.1N_{DGC0}b_1 + N_{MC}b_2 + N_{AC}b_4 + N_{OD}b_5 + N_{MG}b_6 \quad [5]$$
$$c_3 = N_{IN}b_3$$
$$N_{DGC} = (E_{DG} - c_1 - c_2 f_e - c_3 f_i)/(a_1 + 0.127 b_1 f_e).$$

Statistical Analysis. Data were analyzed with Student's *t* tests (paired, two-tailed) and one-way or two-way repeated-measures ANOVA (RM-ANOVA) followed by post hoc Tukey's tests. A value of $P < 0.05$ was considered statistically significant. All data are presented as mean ± SEM and *n* represents the number of neurons unless otherwise specified. Experimental procedures of whole-cell patch recording, immunostaining, and metabolomic and lipidomic analysis are described in *SI Appendix, Supplementary Methods*.

Data Availability. All study data are included in the article and supporting information.

ACKNOWLEDGMENTS. We thank Drs. Simon Halegoua, Hongjun Song, and Greg Kirschen for their critical feedback on this manuscript; and all other members in the S.G. and Q.X. laboratories for their valuable comments.-This work was supported by NIH Grants NS089770, AG046875, NS104868 (to S.G.) and DC016746 (to Q.X.); the National Natural Science Foundation of China (81761128011); partially by the State University of New York Brain Excellence award; the Shanghai Municipal Science and Technology Major Project (No. 2018SHZDZX01) and ZJLab; and the program for the Professor of Special Appointment (Eastern Scholar) at Shanghai Institutions of Higher Learning.

1. G. L. Ming, H. Song, Adult neurogenesis in the mammalian brain: Significant answers and significant questions. *Neuron* **70**, 687–702 (2011).
2. F. H. Gage *et al.*, Survival and differentiation of adult neuronal progenitor cells transplanted to the adult brain. *Proc. Natl. Acad. Sci. U.S.A.* **92**, 11879–11883 (1995).
3. F. H. Gage, Adult neurogenesis in mammals. *Science* **364**, 827–828 (2019).
4. G. A. Pilz *et al.*, Live imaging of neurogenesis in the adult mouse hippocampus. *Science* **359**, 658–662 (2018).
5. K. L. Spalding *et al.*, Dynamics of hippocampal neurogenesis in adult humans. *Cell* **153**, 1219–1227 (2013).
6. M. Boldrini *et al.*, Human hippocampal neurogenesis persists throughout aging. *Cell Stem Cell* **22**, 589–599.e5 (2018).
7. C. D. Clelland *et al.*, A functional role for adult hippocampal neurogenesis in spatial pattern separation. *Science* **325**, 210–213 (2009).
8. N. B. Danielson *et al.*, Distinct contribution of adult-born hippocampal granule cells to context encoding. *Neuron* **90**, 101–112 (2016).
9. V. Ramirez-Amaya, D. F. Marrone, F. H. Gage, P. F. Worley, C. A. Barnes, Integration of new neurons into functional neural networks. *J. Neurosci.* **26**, 12237–12241 (2006).
10. T. Nakashiba *et al.*, Young dentate granule cells mediate pattern separation, whereas old granule cells facilitate pattern completion. *Cell* **149**, 188–201 (2012).
11. J. R. Epp, R. Silva Mera, S. Köhler, S. A. Josselyn, P. W. Frankland, Neurogenesis-mediated forgetting minimizes proactive interference. *Nat. Commun.* **7**, 10838 (2016).
12. S. M. Miller, A. Sahay, Functions of adult-born neurons in hippocampal memory interference and indexing. *Nat. Neurosci.* **22**, 1565–1575 (2019).
13. A. Sahay *et al.*, Increasing adult hippocampal neurogenesis is sufficient to improve pattern separation. *Nature* **472**, 466–470 (2011).
14. V. M. Luna *et al.*, Adult-born hippocampal neurons bidirectionally modulate entorhinal inputs into the dentate gyrus. *Science* **364**, 578–583 (2019).
15. G. Kempermann, H. G. Kuhn, F. H. Gage, More hippocampal neurons in adult mice living in an enriched environment. *Nature* **386**, 493–495 (1997).
16. H. van Praag, G. Kempermann, F. H. Gage, Running increases cell proliferation and neurogenesis in the adult mouse dentate gyrus. *Nat. Neurosci.* **2**, 266–270 (1999).
17. E. Gould, A. Beylin, P. Tanapat, A. Reeves, T. J. Shors, Learning enhances adult neurogenesis in the hippocampal formation. *Nat. Neurosci.* **2**, 260–265 (1999).
18. T. Kobilo *et al.*, Running is the neurogenic and neurotrophic stimulus in environmental enrichment. *Learn. Mem.* **18**, 605–609 (2011).
19. E. H. Park, N. S. Burghardt, D. Dvorak, R. Hen, A. A. Fenton, Experience-dependent regulation of dentate gyrus excitability by adult-born granule cells. *J. Neurosci.* **35**, 11656–11666 (2015).
20. M. Bergami *et al.*, A critical period for experience-dependent remodeling of adult-born neuron connectivity. *Neuron* **85**, 710–717 (2015).
21. J. Shen *et al.*, Neurovascular coupling in the dentate gyrus regulates adult hippocampal neurogenesis. *Neuron* **103**, 878–890.e3 (2019).
22. J. L. Trejo, E. Carro, I. Torres-Aleman, Circulating insulin-like growth factor I mediates exercise-induced increases in the number of new neurons in the adult hippocampus. *J. Neurosci.* **21**, 1628–1634 (2001).
23. L. Cao *et al.*, VEGF links hippocampal activity with neurogenesis, learning and memory. *Nat. Genet.* **36**, 827–835 (2004).
24. S. A. Wolf *et al.*, Cannabinoid receptor CB1 mediates baseline and activity-induced survival of new neurons in adult hippocampal neurogenesis. *Cell Commun. Signal.* **8**, 12 (2010).
25. F. Klempin *et al.*, Serotonin is required for exercise-induced adult hippocampal neurogenesis. *J. Neurosci.* **33**, 8270–8275 (2013).
26. S. Sultan *et al.*, Synaptic integration of adult-born hippocampal neurons is locally controlled by astrocytes. *Neuron* **88**, 957–972 (2015).
27. S. Vicini, The role of GABA and glutamate on adult neurogenesis. *J. Physiol.* **586**, 3737–3738 (2008).
28. S. Ge, D. A. Pradhan, G. L. Ming, H. Song, GABA sets the tempo for activity-dependent adult neurogenesis. *Trends Neurosci.* **30**, 1–8 (2007).
29. K. Jin *et al.*, Neurogenesis and aging: FGF-2 and HB-EGF restore neurogenesis in hippocampus and subventricular zone of aged mice. *Aging Cell* **2**, 175–183 (2003).
30. S. Heigele, S. Sultan, N. Toni, J. Bischofberger, Bidirectional GABAergic control of action potential firing in newborn hippocampal granule cells. *Nat. Neurosci.* **19**, 263–270 (2016).
31. J. Song, R. H. Olsen, J. Sun, G. L. Ming, H. Song, Neuronal circuitry mechanisms regulating adult mammalian neurogenesis. *Cold Spring Harb. Perspect. Biol.* **8**, a018937 (2016).
32. R. T. Káradóttir, C. T. Kuo, Neuronal activity-dependent control of postnatal neurogenesis and gliogenesis. *Annu. Rev. Neurosci.* **41**, 139–161 (2018).
33. C. Y. Yeh *et al.*, Mossy cells control adult neural stem cell quiescence and maintenance through a dynamic balance between direct and indirect pathways. *Neuron* **99**, 493–510.e4 (2018).
34. N. Kee, C. M. Teixeira, A. H. Wang, P. W. Frankland, Preferential incorporation of adult-generated granule cells into spatial memory networks in the dentate gyrus. *Nat. Neurosci.* **10**, 355–362 (2007).
35. G. W. Kirschen *et al.*, Active dentate granule cells encode experience to promote the addition of adult-born hippocampal neurons. *J. Neurosci.* **37**, 4661–4678 (2017).
36. B. Hattiangady, M. S. Rao, A. K. Shetty, Chronic temporal lobe epilepsy is associated with severely declined dentate neurogenesis in the adult hippocampus. *Neurobiol. Dis.* **17**, 473–490 (2004).
37. J. E. Kralic, D. A. Ledergerber, J. M. Fritschy, Disruption of the neurogenic potential of the dentate gyrus in a mouse model of temporal lobe epilepsy with focal seizures. *Eur. J. Neurosci.* **22**, 1916–1927 (2005).
38. A. Sierra *et al.*, Neuronal hyperactivity accelerates depletion of neural stem cells and impairs hippocampal neurogenesis. *Cell Stem Cell* **16**, 488–503 (2015).
39. J. R. Pineda, J. M. Encinas, The contradictory effects of neuronal hyperexcitation on adult hippocampal neurogenesis. *Front. Neurosci.* **10**, 74 (2016).
40. D. D. Alvarez *et al.*, A disynaptic feedback network activated by experience promotes the integration of new granule cells. *Science* **354**, 459–465 (2016).
41. J. Song *et al.*, Parvalbumin interneurons mediate neuronal circuitry-neurogenesis coupling in the adult hippocampus. *Nat. Neurosci.* **16**, 1728–1730 (2013).
42. S. Ge *et al.*, GABA regulates synaptic integration of newly generated neurons in the adult brain. *Nature* **439**, 589–593 (2006).
43. L. Chen, X. Wang, S. Ge, Q. Xiong, Medial geniculate body and primary auditory cortex differentially contribute to striatal sound representations. *Nat. Commun.* **10**, 418 (2019).

44. J. P. Neunuebel, J. J. Knierim, Spatial firing correlates of physiologically distinct cell types of the rat dentate gyrus. *J. Neurosci.* **32**, 3848–3858 (2012).
45. S. Royer *et al*., Control of timing, rate and bursts of hippocampal place cells by dendritic and somatic inhibition. *Nat. Neurosci.* **15**, 769–775 (2012).
46. C. R. Houser, Interneurons of the dentate gyrus: An overview of cell types, terminal fields and neurochemical identity. *Prog. Brain Res.* **163**, 217–232 (2007).
47. H. Hu, J. Gan, P. Jonas, Interneurons. Fast-spiking, parvalbumin^{+} GABAergic interneurons: From cellular design to microcircuit function. *Science* **345**, 1255263 (2014).
48. K. A. Pelkey *et al*., Hippocampal GABAergic inhibitory interneurons. *Physiol. Rev.* **97**, 1619–1747 (2017).
49. N. Guo *et al*., Dentate granule cell recruitment of feedforward inhibition governs engram maintenance and remote memory generalization. *Nat. Med.* **24**, 438–449 (2018).
50. M. G. Vander Heiden, L. C. Cantley, C. B. Thompson, Understanding the Warburg effect: The metabolic requirements of cell proliferation. *Science* **324**, 1029–1033 (2009).
51. R. Beckervordersandforth, Mitochondrial metabolism-mediated regulation of adult neurogenesis. *Brain Plast.* **3**, 73–87 (2017).
52. R. C. Vergara *et al*., The energy homeostasis principle: Neuronal energy regulation drives local network dynamics generating behavior. *Front. Comput. Neurosci.* **13**, 49 (2019).
53. S. Herculano-Houzel, Scaling of brain metabolism with a fixed energy budget per neuron: Implications for neuronal activity, plasticity and evolution. *PLoS One* **6**, e17514 (2011).
54. D. Attwell, S. B. Laughlin, An energy budget for signaling in the grey matter of the brain. *J. Cereb. Blood Flow Metab.* **21**, 1133–1145 (2001).
55. R. G. Shulman, D. L. Rothman, K. L. Behar, F. Hyder, Energetic basis of brain activity: Implications for neuroimaging. *Trends Neurosci.* **27**, 489–495 (2004).
56. G. Yi, W. M. Grill, Average firing rate rather than temporal pattern determines metabolic cost of activity in thalamocortical relay neurons. *Sci. Rep.* **9**, 6940 (2019).
57. K. Saba *et al*., Energetics of excitatory and inhibitory neurotransmission in aluminum chloride model of Alzheimer's disease: Reversal of behavioral and metabolic deficits by Rasa Sindoor. *Front. Mol. Neurosci.* **10**, 323 (2017).
58. A. B. Patel, V. Tiwari, P. Veeraiah, K. Saba, Increased astroglial activity and reduced neuronal function across brain in AβPP-PS1 mouse model of Alzheimer's disease. *J. Cereb. Blood Flow Metab.* **38**, 1213–1226 (2018).
59. S. R. Cobb, E. H. Buhl, K. Halasy, O. Paulsen, P. Somogyi, Synchronization of neuronal activity in hippocampus by individual GABAergic interneurons. *Nature* **378**, 75–78 (1995).
60. Y. Li *et al*., Molecular layer perforant path-associated cells contribute to feed-forward inhibition in the adult dentate gyrus. *Proc. Natl. Acad. Sci. U.S.A.* **110**, 9106–9111 (2013).
61. J. Morstein *et al*., Optical control of sphingosine-1-phosphate formation and function. *Nat. Chem. Biol.* **15**, 623–631 (2019).
62. H. Satsu *et al*., A sphingosine 1-phosphate receptor 2 selective allosteric agonist. *Bioorg. Med. Chem.* **21**, 5373–5382 (2013).
63. R. A. Nicoll, D. Schmitz, Synaptic plasticity at hippocampal mossy fibre synapses. *Nat. Rev. Neurosci.* **6**, 863–876 (2005).
64. L. A. Ewell, M. V. Jones, Frequency-tuned distribution of inhibition in the dentate gyrus. *J. Neurosci.* **30**, 12597–12607 (2010).
65. C. Espinoza, S. J. Guzman, X. Zhang, P. Jonas, Parvalbumin^{+} interneurons obey unique connectivity rules and establish a powerful lateral-inhibition microcircuit in dentate gyrus. *Nat. Commun.* **9**, 4605 (2018).
66. C. T. Lee *et al*., Causal evidence for the role of specific GABAergic interneuron types in entorhinal recruitment of dentate granule cells. *Sci. Rep.* **6**, 36885 (2016).
67. D. GoodSmith *et al*., Spatial representations of granule cells and mossy cells of the dentate gyrus. *Neuron* **93**, 677–690.e5 (2017).
68. V. C. Piatti, L. A. Ewell, J. K. Leutgeb, Neurogenesis in the dentate gyrus: Carrying the message or dictating the tone. *Front. Neurosci.* **7**, 50 (2013).
69. N. A. Cayco-Gajic, R. A. Silver, Re-evaluating circuit mechanisms underlying pattern separation. *Neuron* **101**, 584–602 (2019).
70. Y. Fu *et al*., A cortical circuit for gain control by behavioral state. *Cell* **156**, 1139–1152 (2014).
71. L. Li *et al*., Silent synapses generate sparse and orthogonal action potential firing in adult-born hippocampal granule cells. *eLife* **6**, e23612 (2017).
72. C. V. Dieni *et al*., Low excitatory innervation balances high intrinsic excitability of immature dentate neurons. *Nat. Commun.* **7**, 11313 (2016).
73. S. Ge, C. H. Yang, K. S. Hsu, G. L. Ming, H. Song, A critical period for enhanced synaptic plasticity in newly generated neurons of the adult brain. *Neuron* **54**, 559–566 (2007).
74. A. Marín-Burgin, L. A. Mongiat, M. B. Pardi, A. F. Schinder, Unique processing during a period of high excitation/inhibition balance in adult-born neurons. *Science* **335**, 1238–1242 (2012).
75. S. G. Temprana *et al*., Delayed coupling to feedback inhibition during a critical period for the integration of adult-born granule cells. *Neuron* **85**, 116–130 (2015).
76. E. W. Adlaf *et al*., Adult-born neurons modify excitatory synaptic transmission to existing neurons. *eLife* **6**, e19886 (2017).
77. K. M. McAvoy *et al*., Modulating neuronal competition dynamics in the dentate gyrus to rejuvenate aging memory circuits. *Neuron* **91**, 1356–1373 (2016).
78. B. H. Singer *et al*., Compensatory network changes in the dentate gyrus restore long-term potentiation following ablation of neurogenesis in young-adult mice. *Proc. Natl. Acad. Sci. U.S.A.* **108**, 5437–5442 (2011).
79. Y. Otsu *et al*., Calcium dynamics in astrocyte processes during neurovascular coupling. *Nat. Neurosci.* **18**, 210–218 (2015).
80. G. C. Petzold, D. F. Albeanu, T. F. Sato, V. N. Murthy, Coupling of neural activity to blood flow in olfactory glomeruli is mediated by astrocytic pathways. *Neuron* **58**, 897–910 (2008).
81. V. Rangaraju, N. Calloway, T. A. Ryan, Activity-driven local ATP synthesis is required for synaptic function. *Cell* **156**, 825–835 (2014).
82. A. Trevisiol *et al*., Monitoring ATP dynamics in electrically active white matter tracts. *eLife* **6**, e24241 (2017).
83. W. B. Levy, R. A. Baxter, Energy efficient neural codes. *Neural Comput.* **8**, 531–543 (1996).
84. L. Yu, C. Zhang, L. Liu, Y. Yu, Energy-efficient population coding constrains network size of a neuronal array system. *Sci. Rep.* **6**, 19369 (2016).
85. M. Diamantaki, M. Frey, P. Berens, P. Preston-Ferrer, A. Burgalossi, Sparse activity of identified dentate granule cells during spatial exploration. *eLife* **5**, e20252 (2016).
86. P. Lennie, The cost of cortical computation. *Curr. Biol.* **13**, 493–497 (2003).
87. S. B. Laughlin, Energy as a constraint on the coding and processing of sensory information. *Curr. Opin. Neurobiol.* **11**, 475–480 (2001).
88. M. Yuan *et al*., Somatostatin-positive interneurons in the dentate gyrus of mice provide local- and long-range septal synaptic inhibition. *eLife* **6**, e21105 (2017).
89. T. F. Freund, A. I. Gulyás, Inhibitory control of GABAergic interneurons in the hippocampus. *Can. J. Physiol. Pharmacol.* **75**, 479–487 (1997).
90. A. Kempf *et al*., The sphingolipid receptor S1PR2 is a receptor for Nogo-a repressing synaptic plasticity. *PLoS Biol.* **12**, e1001763 (2014).
91. X. X. Chi, G. D. Nicol, The sphingosine 1-phosphate receptor, $S1PR_1$, plays a prominent but not exclusive role in enhancing the excitability of sensory neurons. *J. Neurophysiol.* **104**, 2741–2748 (2010).
92. C. Li, J. N. Li, J. Kays, M. Guerrero, G. D. Nicol, Sphingosine 1-phosphate enhances the excitability of rat sensory neurons through activation of sphingosine 1-phosphate receptors 1 and/or 3. *J. Neuroinflammation* **12**, 70 (2015).
93. C. H. Yang *et al*., Circuit integration initiation of new hippocampal neurons in the adult brain. *Cell Rep.* **30**, 959–968.e3 (2020).
94. A. Damirin *et al*., Sphingosine 1-phosphate receptors mediate the lipid-induced cAMP accumulation through cyclooxygenase-2/prostaglandin I2 pathway in human coronary artery smooth muscle cells. *Mol. Pharmacol.* **67**, 1177–1185 (2005).
95. D. GoodSmith, H. Lee, J. P. Neunuebel, H. Song, J. J. Knierim, Dentate gyrus mossy cells share a role in pattern separation with dentate granule cells and proximal CA3 pyramidal cells. *J. Neurosci.* **39**, 9570–9584 (2019).
96. J. P. Neunuebel, J. J. Knierim, CA3 retrieves coherent representations from degraded input: Direct evidence for CA3 pattern completion and dentate gyrus pattern separation. *Neuron* **81**, 416–427 (2014).
97. Y. Yu, P. Herman, D. L. Rothman, D. Agarwal, F. Hyder, Evaluating the gray and white matter energy budgets of human brain function. *J. Cereb. Blood Flow Metab.* **38**, 1339–1353 (2018).
98. J. Bielawski, Z. M. Szulc, Y. A. Hannun, A. Bielawska, Simultaneous quantitative analysis of bioactive sphingolipids by high-performance liquid chromatography-tandem mass spectrometry. *Methods* **39**, 82–91 (2006).